Electrochemistry Communications 111 (2020) 106649

Contents lists available at ScienceDirect

Electrochemistry Communications

journal homepage: www.elsevier.com/locate/elecom

Ternary boron-, phosphorus- and oxygen-doped amorphous nickel nanoalloys for enhanced activity towards the oxygen evolution reaction

Xuehui Liu[a], Jian Wu[b,*], Xingjia Guo[a,*]

[a] College of Chemistry, Liaoning University, Shenyang 110036, PR China
[b] Key Laboratory of Magnetic Materials and Devices, Ningbo Institute of Materials Technology and Engineering, Chinese Academy of Sciences, Ningbo 315201, PR China

ARTICLE INFO

Keywords:
Amorphous
Ni nanoalloy
Boron
Phosphorus
Oxygen evolution reaction

ABSTRACT

The oxygen evolution reaction (OER) is a key reaction in hydrogen production through water splitting and in fuel cells. Nickel nanoalloys are potential low-cost OER electrocatalysts, but their catalytic activity and stability need to be improved. The doping of nickel catalysts with anionic elements combined with partial amorphization can improve their electrocatalytic activity. In this study, we report a ternary B-, P- and O-doped amorphous nickel nanoalloy (BPO-Ni) as an effective electrocatalyst for the OER. Compared with binary boron–oxygen-doped nickel (BO-Ni) and phosphorus–oxygen-doped nickel (PO-Ni), ternary BPO-Ni has higher OER catalytic activity and better durability under alkaline conditions. Our results reveal that the high catalytic activity of the B-, P- and O-doped Ni nanoalloy is derived from the synergistic effects between the ternary heteroatoms and the Ni atoms, thereby increasing their catalytic activity. This work produces a new non-metal doped amorphous nickel nanoalloy structure, and offers a way of studying novel inexpensive and efficient OER catalysts.

1. Introduction

Water splitting, one of the most environmentally friendly and effective ways of meeting future global energy demand, involves the hydrogen evolution reaction (HER) and the oxygen evolution reaction (OER) [1]. The sluggish process of four-electron OER is also important for renewable energy applications such as rechargeable metal–air batteries and regenerative fuel cells [2]. However, the OER step requires large overpotentials. Currently, the best electrocatalysts for OER are RuO_2 and IrO_2, but their high cost restrict their large-scale application [3–5]. In recent work, attention has been paid to the development of earth-abundant, low-cost and high-performance metallic materials for OER. Transition metal compounds, including metal oxides, nitride and phosphides, have attracted enormous attention because of their high OER activity [6,7]. Among these transition metal compounds, Ni-based materials are abundant and cheap with excellent catalytic activity for the OER [8–14].

Incorporating other elements into electrocatalysts is a way of improving their electrocatalytic water splitting activities, as this could alter the electronic structure and the surface electronic state [15]. Many studies have reported that boron and phosphorus can affect the catalytic properties of electrocatalysts [16,17]. In particular, nickel borides have been intensively investigated as a result of their unique characteristics, such as low cost, low overpotential and superior stability [18]. Recent reports have shown that Ni-B/Ni foam and Ni-B-O@Ni_3B exhibit effective catalytic activity and stability for both the OER and HER [18,19]. Nickel phosphides have also received much attention as new earth-abundant electrocatalysts. For example, Ni_2P and Ni_5P_4 have been demonstrated to be active toward the OER [13]. Both nickel borides and nickel phosphides exhibit promising OER activity, due to the charge transfer between different elements and their modified electronic structures, thus reducing the kinetic energy barriers to electrochemical processes [20]. In addition, theoretical calculations and experimental studies have shown that the activity of the catalyst is greatly improved if heteroatoms such as N, P, B and S are introduced into the catalyst crystal lattice [15,21,22]. It is therefore reasonable to suppose that Ni-based nanomaterials doped with elements such as B, P and O are likely to be potential OER electrocatalysts [21,23,24].

In the past few decades, amorphous materials have attracted much research attention. Amorphous materials have complicated structures including long-range disorder and short-range order, and high concentrations of unsaturated coordination sites [14,25,26]. Because of these features, it has been demonstrated that electrocatalysts with an amorphous structure have higher activity than those with a crystalline structure [27,28]. Thus, efforts have been made to form and stabilize amorphous structures by incorporating metalloids such as B and P into amorphous alloys, which can affect their electrocatalytic performance [25]. For instance, amorphous Co_2B and CP@Ni-P have been prepared

* Corresponding authors.
E-mail addresses: jwu@nimte.ac.cn (J. Wu), guoxja@sina.com (X. Guo).

https://doi.org/10.1016/j.elecom.2019.106649
Received 10 November 2019; Received in revised form 23 December 2019; Accepted 23 December 2019
Available online 28 December 2019

and found to be highly efficient bifunctional catalysts with stable performance [13,29]. Tuning the crystallinity of electrocatalysts might therefore be an effective way of improving their electrocatalytic performance.

Based on the above analysis, we prepared nickel doped with boron, phosphorus and oxygen (BPO-Ni) using the ice-bath method. Binary boron–oxygen-doped nickel (BO-Ni) and phosphorus–oxygen-doped nickel (PO-Ni) were prepared by the same method. The OER electrocatalytic activity and stability of these catalysts was then studied.

2. Experimental section

2.1. Reagents and chemicals

Nickel chloride hexahydrate ($NiCl_2{\cdot}6H_2O$, 98%), sodium borohydride ($NaBH_4$, 98%), sodium hypophosphite (NaH_2PO_2, 99%), and sodium hydroxide were purchased from the Aladdin Company. All chemicals were used as received without any further purification.

2.2. Preparation of the samples

2.2.1. Synthesis of BO-Ni

The reaction was carried out using Schlenk vacuum equipment under an argon atmosphere. 25 ml of $NaBH_4$ (0.38 g) in 1 M NaOH solution was added to a round-bottomed Schlenk flask and allowed to react under argon for 30 min while the temperature was maintained at 0 °C using an ice bath. 25 ml of an aqueous solution of 0.5 M $NiCl_2{\cdot}6H_2O$ was then added dropwise into the flask. Instantaneous formation of a black sediment could be seen. After 1 h, the black sediment was washed several times with deionized water and dried at 60 °C for 24 h, to produce BO-Ni.

2.2.2. Synthesis of PO-Ni

25 ml of NaH_2PO_2 (0.88 g) in 1 M NaOH solution was added to a round-bottomed Schlenk flask and allowed to react under argon for 30 min while the temperature was maintained at 0 °C using an ice bath. 25 ml of an aqueous solution of 0.5 M $NiCl_2{\cdot}6H_2O$ was then added dropwise into the flask. Instantaneous formation of a grey sediment could be observed. After 1 h, the grey sediment was washed several times with deionized water and dried at 60 °C for 24 h, producing PO-Ni.

2.2.3. Synthesis of BPO-Ni

The steps were similar to the synthesis of BO-Ni, except that 25 ml of both $NaBH_4$ (0.23 g) and NaH_2PO_2 (0.35 g) in 1 M NaOH solution were added to a round-bottomed Schlenk flask (see Fig. S1 in the Supporting Information). BPO-Ni was ultimately obtained.

2.3. Electrochemical measurements

The electrochemical measurements were carried out using a CHI760E electrochemical workstation with a three-electrode setup, including an Ag/AgCl (3 mol/L) reference electrode from BAS instruments, a platinum wire counter electrode and a glassy carbon working electrode. Details of the preparation of the working electrode can be found in Section 1.1 of the Supporting Information (SI).

2.4. Characterization

The three catalysts were characterized by XRD diffraction, transmission electron microscopy (TEM), high-resolution transmission electron microscopy (HRTEM) and scanning electron microscopy (SEM). The synergistic effect of heteroatoms (B, P and O) with Ni atoms was studied by XPS and Raman spectroscopy (for further details see Section 1.2 of the SI).

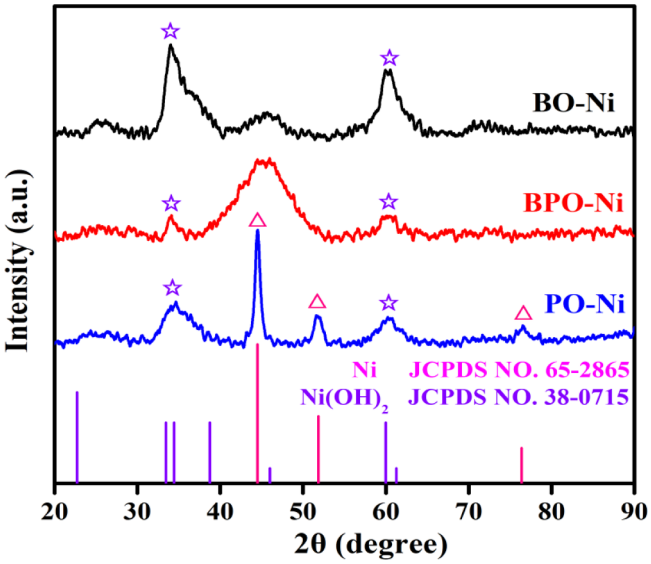

Fig. 1. XRD pattern of BO-Ni, PO-Ni and BPO-Ni.

3. Results and discussion

The XRD diffraction patterns of the BO-Ni, PO-Ni and BPO-Ni electrocatalysts are shown in Fig. 1. For BO-Ni and BPO-Ni, a broad diffraction peak at around 40°–50° demonstrates that both BO-Ni and BPO-Ni contain amorphous states of the nickel–metalloid alloy [16,25,30]. The width of the BPO-Ni broad diffraction peak is broader than that of BO-Ni, indicating that the BPO-Ni is more amorphous than the BO-Ni. For PO-Ni, the diffraction peaks at 44.49, 51.85 and 76.38 can be indexed to the (1 1 1), (2 0 0) and (2 2 0) planes of Ni (JCPDS No. 65-2865). This may be because NaH_2PO_2 is a strong reducing agent and can reduce a salt solution to the metallic state. BO-Ni is more amorphous than PO-Ni because of the atomic sizes and the interaction between Ni and B is much greater than that between Ni and P [30]. BPO-Ni is more amorphous than both BO-Ni and PO-Ni, which may be due to self-structure disturbance by the two metalloids [30]. In addition, the peaks located at around 34° and 60° in all three samples can be attributed to $Ni(OH)_2$ (JCPDS No. 38-0715), consistent with (1 0 1) and (1 1 0) crystalline facets [31].

The morphology and structure of BO-Ni, PO-Ni and BPO-Ni were also characterized by transmission electron microscopy (TEM) and scanning electron microscopy (SEM) as shown in Fig. 2 and Fig. S2. The TEM image shows that BPO-Ni have a spherical morphology and most of the BPO-Ni nanoparticles aggregate together as shapeless particles. From the TEM and SEM images, the average diameter of BPO-Ni particles is about 20–30 nm. Both BO-Ni and PO-Ni have irregular shapes due to the particle agglomeration shown in Fig. S2. Furthermore, HRTEM images and SAED images (Fig. 2c and d) show that BPO-Ni has no obvious lattice fringes, demonstrating that BPO-Ni contains amorphous states of the nickel-metalloid alloy. The sample of BPO-Ni was also studied by elemental mapping, and the images show that B, P and O are uniformly distributed (Fig. S3).

X-ray photoelectron spectroscopy (XPS) was used to investigate the surface chemical compositions and the chemical states of the elements in BO-Ni, PO-Ni and BPO-Ni, and the results are shown in Fig. 3. The Ni 2p spectra for the three samples can be divided into five characteristic peaks. The peaks located at 852.35 (BO-Ni), 851.37 (BPO-Ni), and 850.44 (PO-Ni) can be assigned to metallic Ni (852.7 eV). These three peaks are shifted negatively compared with the pure metallic Ni, which indicates electron transfer from B to metallic Ni [14,16,17,19,30]. The area of metallic Ni in BPO-Ni is larger than in the other two samples. The peaks located at around 855 eV can be ascribed to Ni^{2+}, indicating the presence of surface oxide or hydroxide species [14,20,28,32,33]. As

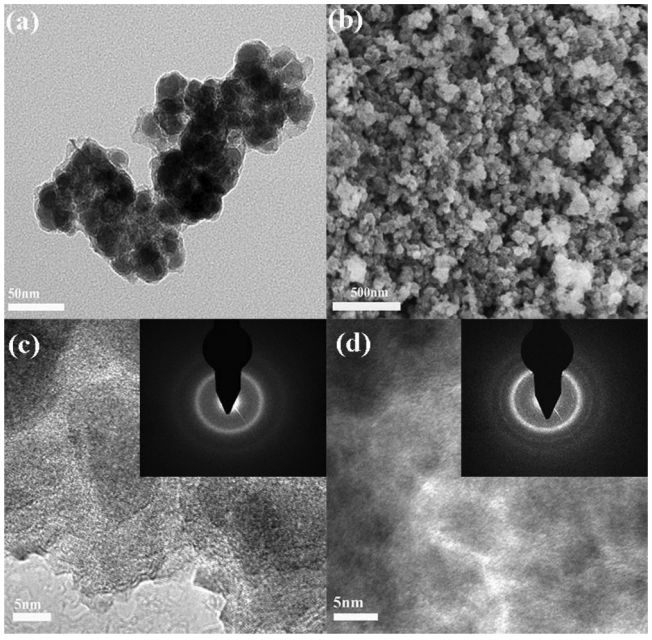

Fig. 2. (a) TEM image of BPO-Ni; (b) SEM image of BPO-Ni; (c and d) HRTEM images of BPO-Ni (inset: SAED patterns of BPO-Ni).

for BPO-Ni, after incorporating B, P and O into the Ni structure, the chemical state of Ni has changed owing to the synergistic promoting effects of the B, P and O elements with the metallic Ni. O 1s can be detected in all three samples and the result is shown in Fig. S4. These results show that all three samples are spontaneously oxidized due to their exposure to air and water, which is consistent with the XRD data.

In the B 1s spectrum, the B 1s can be divided into one peak (191.8 eV) in BO-Ni and two peaks (187.3 and 190.4 eV) in BPO-Ni. The peaks at around 187 eV and 190–192 correspond to the elemental boron and boron oxide species, respectively [16]. The peak at around 187.3 eV is due to the interaction of boron with nickel [22]. The binding energy of BPO-Ni shows a small positive shift compared with the binding energy of pure boron (187.1 eV), indicating that boron gives some electrons to nickel [16]. In the P 2p spectrum, the peaks at 128.3 can be ascribed to nickel interacting with phosphorus and the peaks at around 132 eV can be assigned to oxidized phosphorus. At the same time, the binding energy of BPO-Ni (128.3 eV) shifts negatively compared to red phosphorus (130.4 eV), indicating that phosphorus combines with nickel in BPO-Ni, and phosphorus accepts electrons from nickel [16]. We calculated the element ratios in BO-Ni, PO-Ni and BPO-Ni, respectively. The element ratio of Ni:O:B in BO-Ni is about 3:9:2. The ratio of Ni:O:P in PO-Ni is about 3:9:2. The ratio of Ni:O:B:P in BPO-Ni is about 3:9:1:1. Further evidence of the synergistic effects of the elements B, P and O with metallic Ni, in BO-Ni, BPO-Ni and PO-Ni were provided by Raman spectroscopy. The peaks of BPO-Ni are in agreement with both BO-Ni and PO-Ni peaks, as shown in Fig. S5.

In order to evaluate the electrocatalytic activity of BO-Ni, PO-Ni and BPO-Ni for OER in 1.0 M KOH electrolyte, the three samples were studied by linear sweep voltammetry (LSV) in a standard three-electrode cell at a scan rate of 0.05 V s^{-1}. As shown in Fig. 4a, BO-Ni, PO-Ni and BPO-Ni all display small redox waves (peaks around 1.4 V), which can be attributed to the Ni^{2+}/Ni^{3+} redox process [34,35]. BPO-Ni shows excellent electrocatalytic activity at a higher current density than both BO-Ni and PO-Ni, and the BPO-Ni sample has a current density of up to 10 mA cm^{-2} at 1.60 V vs RHE in KOH (pH = 14). The mass activity (MA, A g^{-1}) was normalized by the total mass loading (0.25 mg cm^{-2}) (see Section S2 and Fig. S6 of the SI). BPO-Ni achieves a high MA of 117.943 A g^{-1} at the η of 0.47 V. In addition, the electrochemical active surface area (ECSA) is

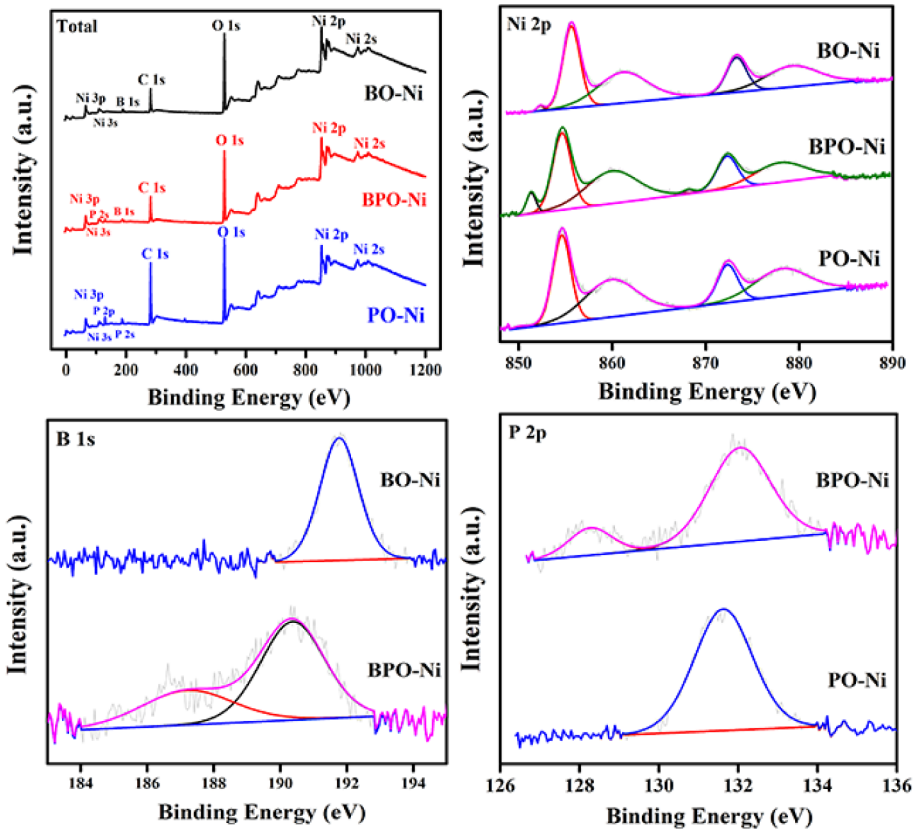

Fig. 3. XPS spectra of BO-Ni, PO-Ni and BPO-Ni; XPS spectra in the Ni 2p regions of BO-Ni, PO-Ni and BPO-Ni; B 1s regions of BO-Ni and BPO-Ni; P 2p regions of PO-Ni and BPO-Ni.

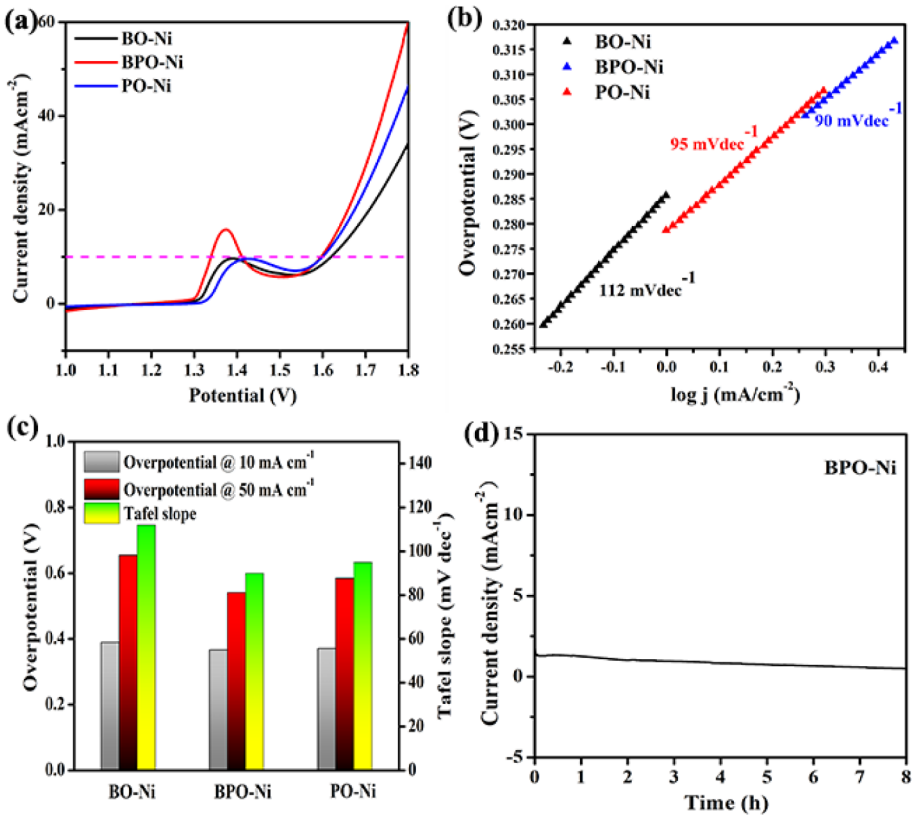

Fig. 4. OER performance: (a) Linear sweep voltammetry (LSV) curves, (b) Tafel plot, (c) Overpotentials required for $J = 10$ mA cm^{-2} and $J = 50$ mA cm^{-2} of BO-Ni, PO-Ni and BPO-Ni in 1.0 M KOH with a scan rate of 0.05 V s^{-1} and Tafel plots for BO-Ni, PO-Ni and BPO-Ni, (d) Amperometric *I-t* curve of BPO-Ni at 1.6 V in 1.0 M KOH for 8 h.

studied by calculating the electrochemical double-layer capacitance (C_{dl}) (see Section S3 and Fig. S7 of the SI). The C_{dl} value of BPO-Ni is 0.665 mF cm^{-2}, which is higher than that of BO-Ni (0.466 mF cm^{-2}) and PO-Ni (0.343 mF cm^{-2}). The result demonstrates that BPO-Ni has more exposed surface reactive sites, which improve the OER activity. Furthermore, the reaction kinetics for OER performance can be evaluated by studying the Tafel plots in an alkaline medium; the Tafel plots for BO-Ni, PO-Ni and BPO-Ni are presented in Fig. 4b. The Tafel slopes are derived from LSV polarization curves obtained at 0.5 mV s^{-1}. The Tafel slope of BPO-Ni is 90 mVdec^{-1}, which is lower than that of BO-Ni (112 mVdec^{-1}) and PO-Ni (95 mVdec^{-1}), respectively. A lower Tafel slope value demonstrates outstanding OER performance with a diminishing overpotential [36]. The OER performance of BPO-Ni is compared with that of some Ni, B and P catalysts reported elsewhere – the corresponding catalytic activity parameters are listed in Table S1. The overpotential of the three samples up to a current density of 10 mA cm^{-2} or 50 mA cm^{-2} and the Tafel slopes are shown in Fig. 4c. It can be concluded that the BPO-Ni catalyst has a lower overpotential and a smaller Tafel slope. The electrocatalytic impedance spectra (EIS) of the three samples were also recorded, with a frequency range from 0.1 Hz to 10^6 Hz, a voltage of 1.60 V and an amplitude voltage of 5 mV (Fig. S8). According to the Nyquist plot, the excellent electrocatalytic activity of BPO-Ni can also be understood in terms of decreasing charge-transfer resistance. Moreover, the long-term stability of catalysts is very important in practical applications. The electrocatalytic stability of BPO-Ni for OER was assessed by chronoamperometry for about 8 h at 1.6 V in 1.0 KOH solution. A stability test (Fig. 4d) indicated that BPO-Ni is a stable catalyst in alkaline conditions at 1.60 V. From these results it can be concluded that BPO-Ni shows a high current density, a small Tafel slope and good stability.

4. Conclusion

In summary, we have shown that B, P and O ternary-doped Ni amorphous nanoalloy (BPO-Ni) is a promising catalyst for OER under alkaline conditions. BPO-Ni has a higher OER activity than BO-Ni and PO-Ni, and an overpotential of 370 mV in 1.0 M KOH. The high OER catalytic performance of BPO-Ni is mainly due to the two factors: firstly, the ternary doping with B, P and O produces a large number of defects and regulates the electronic properties to produce an effective catalytic structure. Secondly, the strong synergistic coupling effect between the B, P, O species and the Ni amorphous nanoalloy further enhances its catalytic activity. This work suggests that synergistic B, P, O species and Ni atoms show great potential as OER catalysts. Thus, the ternary nonmetal (B, P, O)-doped metal Ni nanoalloy offers a promising method of releasing oxygen in renewable energy fields utilizing new and efficient OER catalysts.

Author contributions

Jian Wu and Xuehui Liu prepared the samples and performed measurements and data analysis. The final manuscript has been written by Jian Wu and Xuehui Liu. Jian Wu and Xingjia Guo discussed the results and commented on the manuscript.

Declaration of Competing Interest

The authors declare that they have no known competing financial interests or personal relationships that could have appeared to influence the work reported in this paper.

Acknowledgements

This work is financially supported by National Natural Science Foundation of China (No. 21972156), Natural Science Foundation of Zhejiang Province (No. LY19E010002), Natural Science Foundation of Shaanxi Province (No. 201701D221055) and State Key Laboratory of Special Functional Waterproof Materials (No. SKLW2018006).

Appendix A. Supplementary data

Supplementary data to this article can be found online at https://doi.org/10.1016/j.elecom.2019.106649.

References

[1] J.H. Wang, W. Cui, Q. Liu, Z.C. Xing, A.M. Asiri, X.P. Sun, Recent progress in cobalt-based heterogeneous catalysts for electrochemical water splitting, Adv. Mater. 28 (2016) 215–230.

[2] W.T. Hong, M. Risch, K.A. Stoerzinger, A. Grimaud, J. Suntivich, Y. Shao-Horn, Toward the rational design of non-precious transition metal oxides for oxygen electrocatalysis, Energy Environ. Sci. 8 (2015) 1404–1427.

[3] J. Wu, Y. Xue, X. Yan, W. Yan, Q. Cheng, Y. Xie, Co_3O_4 nanocrystals on single-walled carbon nanotubes as a highly efficient oxygen-evolving catalyst, Nano Res. 5 (2012) 521–530.

[4] J. Wu, G. Wang, J. Du, J.P. Liu, J. Wang, W. Fan, Electrochemical water splitting by pseudo-spinel, disordered and layered lithium nickel oxides: correlation between structural motifs and catalytic properties, ChemCatChem 10 (2018) 2551–2557.

[5] L. Jiao, Y.X. Zhou, H.L. Jiang, Metal-organic framework-based CoP/reduced graphene oxide: high-performance bifunctional electrocatalyst for overall water splitting, Chem. Sci. 7 (2016) 1690–1695.

[6] K.L. Nardi, N. Yang, C.F. Dickens, A.L. Strickler, S.F. Bent, Creating highly active atomic layer deposited NiO electrocatalysts for the oxygen evolution reaction, Adv. Energy Mater. 5 (2015) 1500412.

[7] C. Zhang, J. Liu, Y.X. Ye, Z. Aslam, R. Brydson, C.H. Liang, Fe-N-doped mesoporous carbon with dual active sites loaded on reduced graphene oxides for efficient oxygen reduction catalysts, ACS Appl. Mater. Inter. 10 (2018) 2423–2429.

[8] R. Subbaraman, D. Tripkovic, K.C. Chang, D. Strmcnik, A.P. Paulikas, P. Hirunsit, M. Chan, J. Greeley, V. Stamenkovic, N.M. Markovic, Trends in activity for the water electrolyser reactions on 3d M(Ni Co, Fe, Mn) hydr(oxy)oxide catalysts, Nat. Mater. 11 (2012) 550–557.

[9] M.R. Gao, W.C. Sheng, Z.B. Zhuang, Q.R. Fang, S. Gu, J. Jiang, Y.S. Yan, Efficient water oxidation using nanostructured alpha-nickel-hydroxide as an electrocatalyst, J. Am. Chem. Soc. 136 (2014) 7077–7084.

[10] W.J. Zhou, X.J. Wu, X.H. Cao, X. Huang, C.L. Tan, J. Tian, H. Liu, J.Y. Wang, H. Zhang, Ni_3S_2 nanorods/Ni foam composite electrode with low overpotential for electrocatalytic oxygen evolution, Energy Environ. Sci. 6 (2013) 2921–2924.

[11] B. You, N. Jiang, M.L. Sheng, M.W. Bhushan, Y.J. Sun, Hierarchically porous urchin-like Ni_2P superstructures supported on nickel foam as efficient bifunctional electrocatalysts for overall water splitting, ACS Catal. 6 (2016) 714–721.

[12] A.T. Swesi, J. Masud, M. Nath, Nickel selenide as a high-efficiency catalyst for oxygen evolution reaction, Energy Environ. Sci. 9 (2016) 1771–1782.

[13] X. Wang, W. Li, D. Xiong, D.Y. Petrovykh, L. Liu, Bifunctional nickel phosphide nanocatalysts supported on carbon fiber paper for highly efficient and stable overall water splitting, Adv. Funct. Mater. 26 (2016) 4067–4077.

[14] X.P. Wen, H.B. Dai, L.S. Wu, P. Wang, Electroless plating of Ni–B film as a binder-free highly efficient electrocatalyst for hydrazine oxidation, Appl. Surf. Sci. 409 (2017) 132–139.

[15] B.K. Kim, S.K. Kim, S.K. Cho, J.J. Kim, Enhanced catalytic activity of electro-deposited Ni-Cu-P toward oxygen evolution reaction, Appl. Catal. B Environ. 237 (2018) 409–415.

[16] W.J. Wang, J.H. Shen, Y.W. Chen, Hydrogenation of p-chloronitrobenzene on Ni-P-B nanoalloy catalysts, Ind. Eng. Chem. Res. 45 (2006) 8860–8865.

[17] J. Masa, C. Andronescu, H. Antoni, I. Sinev, S. Seisel, K. Elumeeva, S. Barwe, S. Marti-Sanchez, J. Arbiol, B. Roldan Cuenya, M. Muhler, W. Schuhmann, Role of boron and phosphorus in enhanced electrocatalytic oxygen evolution by nickel borides and nickel phosphides, ChemElectroChem 6 (2019) 235–240.

[18] W. Yuan, X. Zhao, W. Hao, J. Li, L. Wang, X. Ma, Y. Guo, Performance of surface-oxidized Ni_3B, Ni_2B, and NiB_2 electrocatalysts for overall water splitting, ChemElectroChem 6 (2019) 764–770.

[19] Y. Liang, X. Sun, A.M. Asiri, Y. He, Amorphous Ni-B alloy nanoparticle film on Ni foam: rapid alternately dipping deposition for efficient overall water splitting, Nanotechnology 27 (2016) 12LT01.

[20] J.M.V. Nsanzimana, Y. Peng, Y.Y. Xu, L. Thia, C. Wang, B.Y. Xia, X. Wang, An efficient and earth-abundant oxygen-evolving electrocatalyst based on amorphous metal borides, Adv. Energy Mater. 8 (2018) 1701475.

[21] X. Zheng, J. Wu, X. Cao, J. Abbott, C. Jin, H. Wang, P. Strasser, R. Yang, X. Chen, G. Wu, N-, P-, and S-doped graphene-like carbon catalysts derived from onium salts with enhanced oxygen chemisorption for Zn-air battery cathodes, Appl. Catal. B Environ. 241 (2019) 442–451.

[22] P. Zhang, X. Sheng, X. Chen, Z. Fang, J. Jiang, M. Wang, F. Li, L. Fan, Y. Ren, B. Zhang, B.J.J. Timmer, M.S.G. Ahlquist, L. Sun, Paired electrocatalytic oxygenation and hydrogenation of organic substrates with water as the oxygen and hydrogen source, Angew. Chem. Int. Edit. 58 (2019) 9155–9159.

[23] C.H. Choi, S.H. Park, S.I. Woo, Binary and ternary doping of nitrogen, boron, and phosphorus into carbon for enhancing electrochemical oxygen reduction activity, ACS Nano 6 (2012) 7084–7091.

[24] S. Zhao, J. Liu, C. Li, W. Ji, M. Yang, H. Huang, Y. Liu, Z. Kang, Tunable ternary (N, P, B)-doped porous nanocarbons and their catalytic properties for oxygen reduction reaction, ACS Appl. Mater. Inter. 6 (2014) 22297–22304.

[25] X. Yin, Q. Wang, D. Duan, S. Liu, Y. Wang, Amorphous NiB alloy decorated by Cu as the anode catalyst for a direct borohydride fuel cell, Int. J. Hydrogen Energy 44 (2019) 10971–10981.

[26] D. He, L. Zhang, D. He, G. Zhou, Y. Lin, Z. Deng, X. Hong, Y. Wu, C. Chen, Y. Li, Amorphous nickel boride membrane on a platinum-nickel alloy surface for enhanced oxygen reduction reaction, Nat. Commun. 7 (2016) 12362.

[27] W.J. Jiang, S. Niu, T. Tang, Q.H. Zhang, X.Z. Liu, Y. Zhang, Y.Y. Chen, J.H. Li, L. Gu, L.J. Wan, J.S. Hu, Crystallinity-modulated electrocatalytic activity of a nickel(II) borate thin layer on Ni_3B for efficient water oxidation, Angew. Chem. Int. Edit. 56 (2017) 6572–6577.

[28] M. Zhou, Q. Sun, Y. Shen, Y. Ma, Z. Wang, C. Zhao, Fabrication of 3D microporous amorphous metallic phosphides for high-efficiency hydrogen evolution reaction, Electrochim. Acta 306 (2019) 651–659.

[29] J. Masa, P. Weide, D. Peeters, I. Sinev, W. Xia, Z. Sun, C. Somsen, M. Muhler, W. Schuhmann, Amorphous cobalt boride (Co_2B) as a highly efficient nonprecious catalyst for electrochemical water splitting: oxygen and hydrogen evolution, Adv. Energy Mater. 6 (2016) 1502313.

[30] H. Li, Q. Zhao, H. Li, Selective hydrogenation of p-chloronitrobenzene over Ni–P–B amorphous catalyst and synergistic promoting effects of B and P, J. Mol. Catal. A-Chem. 285 (2008) 29–35.

[31] S.H. Tang, L.P. Sui, Z. Dai, Z.T. Zhu, H.X. Huangfu, High supercapacitive performance of $Ni(OH)_2$/XC-72 composite prepared by microwave-assisted method, RSC Adv. 5 (2015) 43164–43171.

[32] J. Masa, I. Sinev, H. Mistry, E. Ventosa, M. de la Mata, J. Arbiol, M. Muhler, B. Roldan Cuenya, W. Schuhmann, Ultrathin high surface area nickel boride (Ni_xB) nanosheets as highly efficient electrocatalyst for oxygen evolution, Adv. Energy Mater. 7 (2017) 1700381.

[33] F. El Gabaly, K.F. McCarty, H. Bluhm, A.H. McDaniel, Oxidation stages of Ni electrodes in solid oxide fuel cell environments, Phys. Chem. Chem. Phys. 15 (2013) 8334–8341.

[34] M.W. Louie, A.T. Bell, An investigation of thin-film Ni-Fe oxide catalysts for the electrochemical evolution of oxygen, J. Am. Chem. Soc. 135 (2013) 12329–12337.

[35] L.A. Stern, X.L. Hu, Enhanced oxygen evolution activity by NiO_x and $Ni(OH)_2$ nanoparticles, Faraday Discuss. 176 (2014) 363–379.

[36] Y. Zhao, X. Jia, G. Chen, L. Shang, G.I. Waterhouse, L.Z. Wu, C.H. Tung, D. O'Hare, T. Zhang, Ultrafine NiO nanosheets stabilized by TiO_2 from monolayer NiTi-LDH precursors: an active water oxidation electrocatalyst, J. Am. Chem. Soc. 138 (2016) 6517–6524.